Physical Modelling of Rainfall-Induced Sandy and Clay-Like Slope Failures

Vivoda Prodan, Martina; Peranić, Josip; Pajalić, Sara; Arbanas, Željko

Hindawi
Advances in Materials Science and Engineering
Volume 2023, Article ID 3234542, 12 pages
https://doi.org/10.1155/2023/3234542

Research Article

Physical Modelling of Rainfall-Induced Sandy and Clay-Like Slope Failures

Martina Vivoda Prodan, Josip Peranić, Sara Pajalić, and Željko Arbanas

Faculty of Civil Engineering, University of Rijeka, Radmile Matejčić 3, 51000 Rijeka, Croatia

Correspondence should be addressed to Martina Vivoda Prodan; martina.vivoda@gradri.uniri.hr

Received 29 September 2022; Revised 20 December 2022; Accepted 13 January 2023; Published 6 February 2023

Academic Editor: Qian Chen

Small-scale slope modelling was performed to evaluate the failure process of a landslide triggered by artificial rainfall. The model platform 2.3 m long, 1.0 m wide, and 0.5 m deep was used to build small-scale slope models with the same geometric conditions but different soil types/materials, including sand and two sand-kaolin mixtures with the same slope angle. The hydraulic response of the slope models under simulated rainfall conditions was monitored using volumetric water content, pore water pressure, and matric suction sensors installed at different depths and along different profiles. Slope surface deformation and failure development was also monitored. This paper discusses the factors affecting landslide initiation and propagation, and their relationship to the slope material, infiltration process, and overall soil resistance in a slope related to soil strength, effective stress, and matric suction contribution in the unsaturated part of the slope. Rainfall infiltration caused increase of volumetric water content, dissipation of suction in initially partially saturated materials of the small-scale slope models, resulting in a decrease in effective stresses and shear strength, which in turn led to the occurrence of movements and initiation of slope failures. The main observations arising from the results of the conducted tests relate to initiation and development of the observed instabilities of sandy and clay-like slopes. The test results have shown that within the slopes built from clean sand failure occurs due to groundwater level rising at the slope foot and further retrogressive failure towards the top of the slope, while in the slopes built from sand-kaolin mixtures, instabilities occur in the form of cracks in unsaturated conditions and are the result of matric suction dissipation due to rainfall infiltration.

1. Introduction

The landslides are hazardous motions of a mass of rock, Earth, or debris down the slope, under the influence of gravity [1] that pose a serious threat to the population all around the world [2]. The most frequent and widespread damaging landslides are induced by prolonged or heavy rainfall. Rainfall is the most relevant factor for the triggering of both shallow and deep-seated landslides, and rainfall analysis is the most frequently adopted approach for forecasting the occurrence of such phenomena. Therefore, the prediction of rainfall-induced landslides constitutes one of the key scientific questions with significant social implications.

To model the relationship between rainfall and slope stability, different approaches have been generally used. For a long time, landslide modelling was based only on numerical modelling results using soil strength parameters obtained from soil laboratory testing in conventional laboratory devices or obtained from the slope stability back-analysis results. Numerical models to investigate behaviour of both shallow and deep-seated landslides triggered by rainfall have been studied (e.g., [3–8]). Direct measurement of pressures and displacements in real slopes is only possible for monitored sites during the occurrence of landslides and artificially induced failure in real slopes, and in both cases, measurements are not repeatable. Direct observation of pore water pressures and stresses in landslides artificially induced can be performed by physical modelling in the laboratory.

The physical modelling of landslide processes can create well documented, highly-instrumented case-studies of slope

behaviour in which the material properties, initial state, and boundary conditions are precisely defined. Physical modelling of landslide behaviour using small-scale models was introduced as a solution in different landslide research studies in 1970 s and 1980 s in Japan [9, 10] on natural slopes exposed to artificial rainfall. Laboratory experiments on landslide behaviour in a scaled physical model began in the 1980 s in Canada [11], Japan [12], and Australia [13] under 1 g conditions. Small-scale landslide modelling under increased acceleration in a geotechnical centrifuge has also been successfully adopted (e.g., [14, 15]) but under circumstances of centrifuge limitations. Scale effects are significant in small-scale physical models of landslides, and Iverson [16] reduced them by performing a full-scale flume test. Small- or large-scale physical landslide models have been successfully used in combination with advanced monitoring techniques and appropriate sensor networks, to study the infiltration process, landslide initiation, and the propagation phase of landslides triggered by artificial rainfall under 1 g conditions. Numerous physical models have been investigated infiltration behaviour during rainfall on different materials. Wang and Sassa [17] performed a series of tests to trigger rainfall-induced landslides using a small flume built from silica sand no. 7, no. 8, and mixtures of silica sand no. 8 with different contents of loess. They concluded that grain size and fine-particle contents can have a significant impact on the mobility of rainfall-induced landslides. Moriwaki et al. [18] conducted a full-scale failure experiment triggered by rainfall using a laboratory slope built from a loose sandy soil. It was inferred that the increased water pressures in the upper slope resulted from collapse of loose soil structure during shearing in the translational slide, whereas those in the lower portion of the slope and horizontal sections resulted from a mix of soil compression and shearing by the sliding mass. To develop physically based warning system for rainfall-induced slope failures, Tohari et al. [19] performed a series of laboratory experiments on two different sandy soils—river sand and residual granite soil. The results of model tests showed that failures of the model slopes were essentially initiated by the development of an unstable area near the slope toe, upon the formation of the seepage area, with shallow noncircular sliding being the dominant failure mode. The volumetric moisture content of the slope region where localized failures initiated was noted to reach a nearly saturated value. However, the major portion of soil slopes involved in overall instability was still in an unsaturated condition. Precise monitoring of the change in the moisture content can provide the possibility of developing a reliable and effective means for predicting failure or issuing hazard warning of slope failures, during a particular rainfall. Olivares et al. [20] investigated the mechanics of flow slides in cohesionless pyroclastic soils using a full-scale flume test. They described the instrumented flume and the procedures adopted for monitoring the major aspects of slope behaviour to understand the mechanisms of infiltration and to assess the soil suction distribution in such layered deposits. To identify the most useful variables to be monitored for building up effective early warning systems, Greco et al. [21] conducted infiltration experiments in instrumented model slopes, made up of a single layer of loose granular pyroclastic soil, until the occurrence of slope failure. Monitoring of soil volumetric water content seemed more useful than soil suction monitoring for early warning purposes, since water content grew smoothly during the entire infiltration processes, while soil suction showed abrupt steep fronts. Montrasio et al. [22] performed numerous flume tests to analyse the triggering process of soil slips and to verify the reliability of SLIP, a simplified stability model that is able to predict the occurrence of these phenomena. They consider that the experimental tests, excluding the laboratory and scale effects, reproduce as accurately as possible the site conditions, on the basis of the obtained results, and they suggest that the model can be a useful tool for shallow landslide susceptibility assessment even at the regional scale. Damiano et al. [23] carried out infiltration experiment in three-layered small-scale slopes of pyroclastic deposits. The results highlight that the presence of coarse-textured unsaturated pumiceous layers, interbedded between finer ashy layers, can delay the wetting front advancement, thus initially confining the infiltration process within the uppermost finer layer. A diversion of the flow from the vertical towards the slope direction occurs when the soil approaches saturation. However, whereas a high hydraulic gradient establishes across pumices, water infiltration into the deepest layer begins, and part of the water crosses the pumices, before the complete saturation of the uppermost soil profile. Chueasamat et al. [24] investigated the effects of surface sand layer density and rainfall intensity on the slope failures due to rainfalls using 1 g physical slope models constructed of sand and silt soil. They concluded that the difference of generation mechanism of PWP values may be the deciding factor in the difference in the type of failure. An instrumented flume of a homogeneous slope of pyroclastic soil was analysed by Spolverino et al. [25]. The test showed that the role of suction and soil density was essential for this type of soil and that failure occurred when the suction was close to zero, reducing the effects of apparent cohesion, while density strongly conditioned the dynamics with which the instability manifested itself. Thickened soil did not allow a mudflow to occur. A flume test on weathered soil was conducted by Lee et al. [26] to evaluate the failure mechanism of a rainfall-induced landslide and to develop a physically based warning system. The results showed that rainfall infiltration into the partially saturated soil gradually increased the volumetric water content and decreased the matric suction, resulting in decrease of the soil strength and soil deformation and landslide occurrence. The matric suction and the degree of saturation were used to calculate the generalized effective stress of the solid to develop a warning system. The authors discussed that the inflection point of the stress paths can be used to define threshold for a rainfall-induced landslide warning system. Yang et al. [27] validated numerical model by comparing the predicted displacement with those measured from a full-scale landslide flume test. The numerical results indicated that the slope deformation characteristics are influenced by various hydrological and geological factors.

This paper describes small-scale landslide modelling under 1 g loading conditions. The main task of landslide physical modelling was to study the initiation, propagation, and accumulation of landslides caused by infiltration of rainfall into the slope by monitoring the volumetric water content and matric suction in the slope. This research was conducted within the four-year research project "Physical modelling of landslide remediation constructions' behaviour under static and seismic actions" at the University of Rijeka, Croatia, funded by the Croatian Science Foundation [28]. The paper gives an overview of the methods and monitoring equipment used in the physical models of a slope exposed to artificial rainfall. The hydraulic response of a sandy and clay-like scaled slopes exposed to artificial rainfall was monitored using pore water pressure and soil moisture sensors. The results are presented and analysed in this paper.

2. Physical Model

The main objective of the Project was modelling and analysing behaviour of landslide remedial measures in physical models of scaled landslides under static [29–40] and seismic conditions. The platform for testing of downscaled slope models was designed to enable the initiation of landslides by controlled artificial rainfall and equipped with adequate photogrammetric equipment and a complex sensor network within a slope. The series of tests described in this paper were carried out on a slope inclination of 35° with three different soil type materials.

2.1. Model Platform. The model platform was made of steel elements and plates, while the side walls consisted of transparent plexiglass panels to ensure that movements can be both observed and filmed during the test. The platform was 0.5 m high, 1.0 m wide, while the upper, middle, and lower sections were 0.3, 1.4 m, and 0.8 m long, respectively. Slope inclination could be varied from 20° to 45° with the adjustable upper part of the model. The total depth of soil material in all slope models was adopted to be 30 cm. To prevent possible sliding of the soil mass at the contact with the model base, the geogrid mesh was fixed to the platform base to increase friction. Liquid rubber and silicone were used to seal small gaps between plexiglass walls and perforations in the structure. Drainage pipes were installed in the lower part of the model to control the water level during the test and to drain the water after the test [31]. Figure 1 shows the model platform after the installation of the material and monitoring equipment.

2.2. Soil Material Properties and Placement. Three different and simple soil materials were selected to build in the small-scale physical model: sand (S) and sand-kaolin mixture with 10% (SK10) and 15% (SK15) kaolin content. The fine-grained (0-1 mm) Drava River sand was chosen as the base material to represent cohesionless slopes. Another material was a mixture of the base material with 10% and 15% by mass of industrial kaolin and represents the behaviour of fine-grained, cohesive materials with stable cohesion. Kaolin was chosen as clay with low plasticity and a relatively well-graded grain size distribution curve and is not too sensitive to changes in water content. The sand-kaolin mixtures were prepared by adding a predetermined amount of dry kaolin to dry sand (gravimetrically) and then mixing thoroughly with a laboratory mixer. During or before mixing, the amount of clean water was also poured into the soil mixture to achieve the desired initial soil moisture content. Once a homogeneous mixture was achieved, the material was placed in plastic bags, sealed, and left to rest until the model was built. The Mohr–Coulomb strength parameters of the described materials-friction angle and cohesion were determined in a direct shear device at low normal stresses similar to those in the small-scale slope model. Mohr–Coulomb failure envelopes are shown in Figure 2(a). Grain size distribution curves were determined using combination of sieving and sedimentation (hydrometer) analysis according to ASTM D7928, and are presented in Figure 2(b). The hydraulic conductivity was determined using the constant and falling head test methods in oedometer and triaxial apparatuses. The ASTM standard method D854-14 2014 was used to obtain specific gravity of solid soil particles using water pycnometer. The basic physical and mechanical properties of the described materials and the targeted initial conditions at the start of the tests are given in Table 1.

The three materials previously described were used to build slope models with an inclination of 35°, by compacting 5 layers, each 6 cm thick, until a 30 cm high slope was completed. The prepared S material with a water content of $w = 2\%$ and the SK10 and SK15 material with a water content of $w = 5\%$ and $w = 8.1\%$, respectively, were placed using the under-compaction method [41]. The installation of the material at the targeted initial water contents ensured homogeneous conditions within the slope models in terms of overall density at the start of the tests. The higher initial water content for the sand-kaolin mixture was required for effective compaction, as previously determined by the Proctor test. The initial water content could not be maintained during the sandy slope model construction; model construction extends over several days and evaporation and internal redistribution of water content are the reasons for the nonuniform water content distribution in a model at the start of the test. Soil moisture conditions were reached during model construction and kept constant until the start of the tests on the clay-like slopes [39]. Each layer was compacted by hand compactor to the medium dense conditions of relative density $Dr = 50\%$ for S and SK10 slopes. To reduce the effects of volumetric deformation when the soil is wetted and to facilitate placement and compaction during model construction, SK15 mixture was placed with a higher relative density ($Dr = 75\%$) and a target soil moisture content of 8.1%. Before placing the next layer, the surface of the previous layer was raked and sprayed with a small amount of water to maintain the initial moisture content and achieve good contact between the particles of the two layers. The slope model was divided into three segments—the upper (H), middle (M), and lower (L). To facilitate the placement of the soil material, care was taken during compaction of the

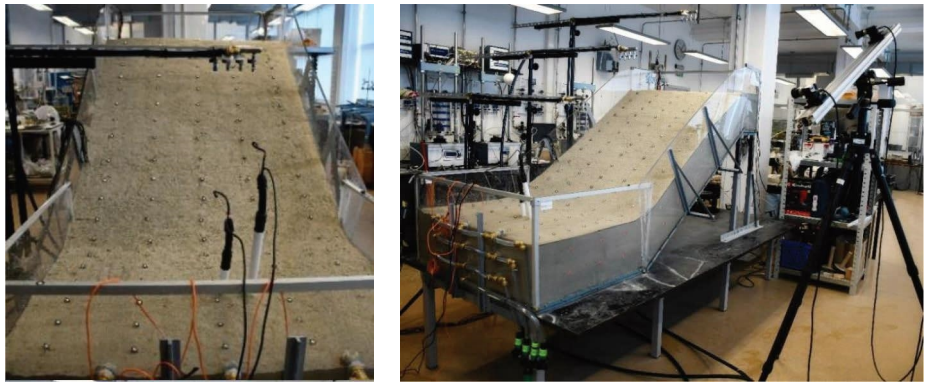

(a) (b)

Figure 1: Photo of the small-scale landslide model at 35°: (a) front view; (b) side view.

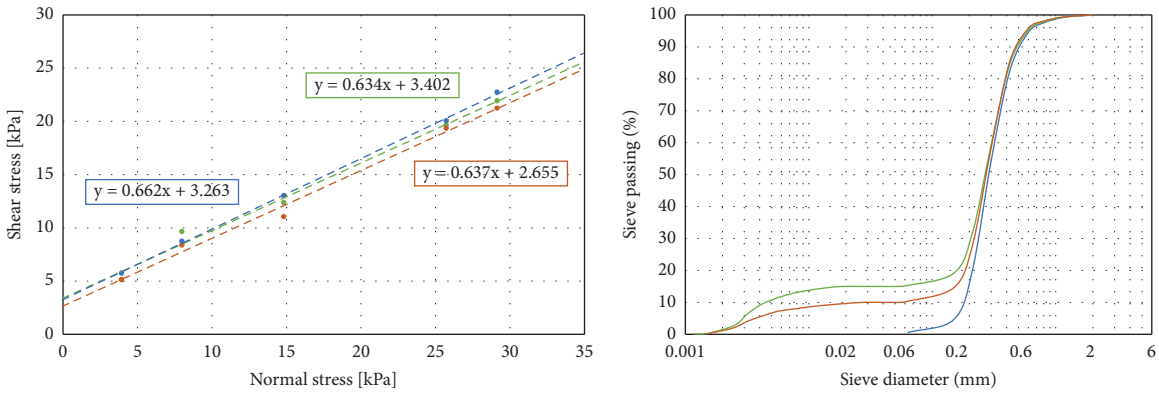

(a) (b)

Figure 2: (a) Mohr–Coulomb failure envelopes and (b) grain size distribution curves of S (blue), SK10 (orange), and SK15 (green).

Table 1: Basic physical and mechanical properties of the S and sand-kaolin mixture SK10 and SK15 built in the small-scale model and the initial conditions at the start of a test [37].

Parameters	Sand (S)	*Sand-kaolin mixture*	
		Sand + 10% kaolin (SK10)	Sand + 15% kaolin (SK15)
Specific gravity, *Gs*	2.70	2.69	2.67
Dry density, ρ_d (g/cm^3)	1.52	1.43	1.51
Total density, ρ_t (g/cm^3)	1.55	1.50	1.63
Effective particle size			
D_{10} (mm)	0.19	0.038	0.056
D_{60} (mm)	0.37	0.31	0.207
Uniformity coefficient, c_u	1.947	8.16	54.107
Minimum void ratio, e_{min}	0.641	0.647	0.544
Maximum void ratio, e_{max}	0.911	1.121	1.430
Hydraulic conductivity, k_s (m/s)	$1E-05$	$6.78E-06$	$3.5E-06$
Friction angle, ϕ (°)	33.5	32.5	32.4
Cohesion, c (kPa)	0	2.7	3.4
Initial porosity, n_i	0.44	0.469	0.434
Initial void ration, e_i	0.78	0.884	0.766
Initial relative density, D_{ri}	0.5	0.5	0.75
Initial water content, w_i (%)	2	5	8.1

soil layers to ensure that lower segment consisted of one more layer of soil than the upper segment during the construction of the model. For example, a layer from segment M was not placed until the second layer in segment L was finished. The next step was to place the third layer in segment L, the second in segment M, and then, the first layer

of segment H. After compaction of each soil layer was completed, the sensors were placed at predefined locations of one of the three measurement profiles in segments L, M, or H, as described in the following part.

2.3. Monitoring Equipment. The monitoring system established in a physical model followed the principles used in the observation of real landslides and consisted of a geotechnical and a geodetic monitoring system.

The geotechnical monitoring system comprised of a complex network of miniature sensors equivalent to the geotechnical monitoring devices used in the field [42]. Thus, accelerometers, soil water content sensors, mini tensiometers, and pore-pressure transducers were installed to measure soil moisture, pore pressure, displacements, and matric suction. All sensors used in the tests were constantly connected to data loggers for continuous data collection during the time of the test. Installation of the measuring sensors was performed parallel to the soil layers after compaction was completed. The water-related sensors (Figure 3) that are the focus of this paper were TEROS 10 and TEROS 12 frequency-domain reflectometry-based soil moisture sensors which provided an indirect measurement of the volumetric water content of porous materials installed in all three tests, while the TEROS 31 mini tensiometers and the TEROS 21 maintenance-free matric potential sensor for measurement of soil water potential were used only in the tests with sand-kaolin mixtures. All the aforementioned sensors were manufactured by the METER Group AG (Munich, Germany). The locations of the sensors were chosen as critical points for monitoring the hydromechanical response of slope models. The sensors were installed in the lower (L), middle (M), and upper (H) part of the slope, on different depths of 6, 12, 18, and 24 cm along the same profile to provide data at the same cross-section that enables validation and numerical analysis of the observed landslide initiation. Similar types of sensors to monitor volumetric water content and soil potential in small-scale model were used by Huang and Chien [43] and Wu et al. [44]. A detailed description of the equipment used in the geotechnical monitoring system is described in Pajalić et al. [31] and Peranić et al. [39, 40].

The geodetic monitoring system was based on an innovative photogrammetric equipment for multitemporal landslide analysis [45] of image sequences obtained by a pair of high-speed stereo cameras. Terrestrial laser scanning (TLS) and structure-from-motion (SfM) photogrammetry surveys allowed determination of the slope model surface at the beginning and end of the test.

2.4. Rainfall Simulator. The landslide initiation and motion caused by rainfall infiltration in the small-scale model was fully controlled by the rainfall simulator constructed as part of the project. The rainfall simulator consisted of three sprinkler branches, each equipped with four different axial-flow full-cone nozzles with a spray angle of 60° or 90°. Each branch has been placed approximately 0.8 m above the model material. A wide range of rainfall intensities and the possibility to change the location of the rainfall by opening or closing valves on each of the branches allowed modelling of different rainfall patterns and different rainfall intensities applied to the slope model [29, 31].

3. Testing Results

After installing the soil and monitoring equipment within the slope model, the slope models were exposed to artificial rainfall from three nozzles (Figure 4(a)), each delivering the rainfall to one part of the slope—upper (H), middle (M), and lower (L). The slopes were exposed to different rainfall intensities (Figure 4(b)). The rainfall intensity on the sandy slopes was 82 mm/h, while the slopes built of sand-kaolin mixture with 10% and 15% mass of kaolin had an intensity of 33 mm/h. The rainfall intensities were chosen based on infiltration conditions, with the main requirement being that all water at the point of contact on the model surface infiltrate without causing surface runoff. The applied intensities were in the upper range of rainfall infiltration capacity.

The basic data of the three tests performed are presented in Table 2. Test 1 used clean sand (S), while the mixture of sand with 10% of mass of kaolin (SK10) was used in Test 2 and mixture of sand with 15% of mass of kaolin (SK15) in Test 3. After the initial establishment of constant rainfall intensity and a stable infiltration process, the models were subjected to constant rainfall intensity until the slope failed or until the end of the test was declared. The time from the rainfall start to the first signs of instability was 56 minutes for clean sand in Test 1 (Figure 5(a)), while the same was observed after 24 and 35 minutes in Test 2 and Test 3, respectively (Figures 5(d) and 5(g)). The end of the test was declared when further retrogressive sliding was no longer possible: after 126 minutes for the S slope material (Figure 5(c)), and after 155 and 245 minutes for the slopes built of SK10 and SK15, respectively (Figures 5(f) and 5(i)).

The presented superficial signs of instabilities as well as causes of their occurrence in all three tests can be explained from the detailed volumetric water content (VWC) records obtained from soil moisture sensors, shown in Figure 6, and measurements of matric suction obtained from tensiometers, shown in Figure 7.

4. Discussion

Analysis of the measured results of change in volumetric water content (VWC) and matric suction within the slope were performed to investigate the effects of rainwater infiltration and groundwater level (GWL) rise process on the hydromechanical response of the slope models. Knowledge of these processes provides better understanding of landslide initiation. The observed modes of failure in all tests are also discussed.

4.1. Modes of Failure. In Test 1, conducted on the sandy slope, the slope remained stable until the groundwater level reached the slope surface at the foot of the slope and consequently caused a decrease in the soil shear strength.

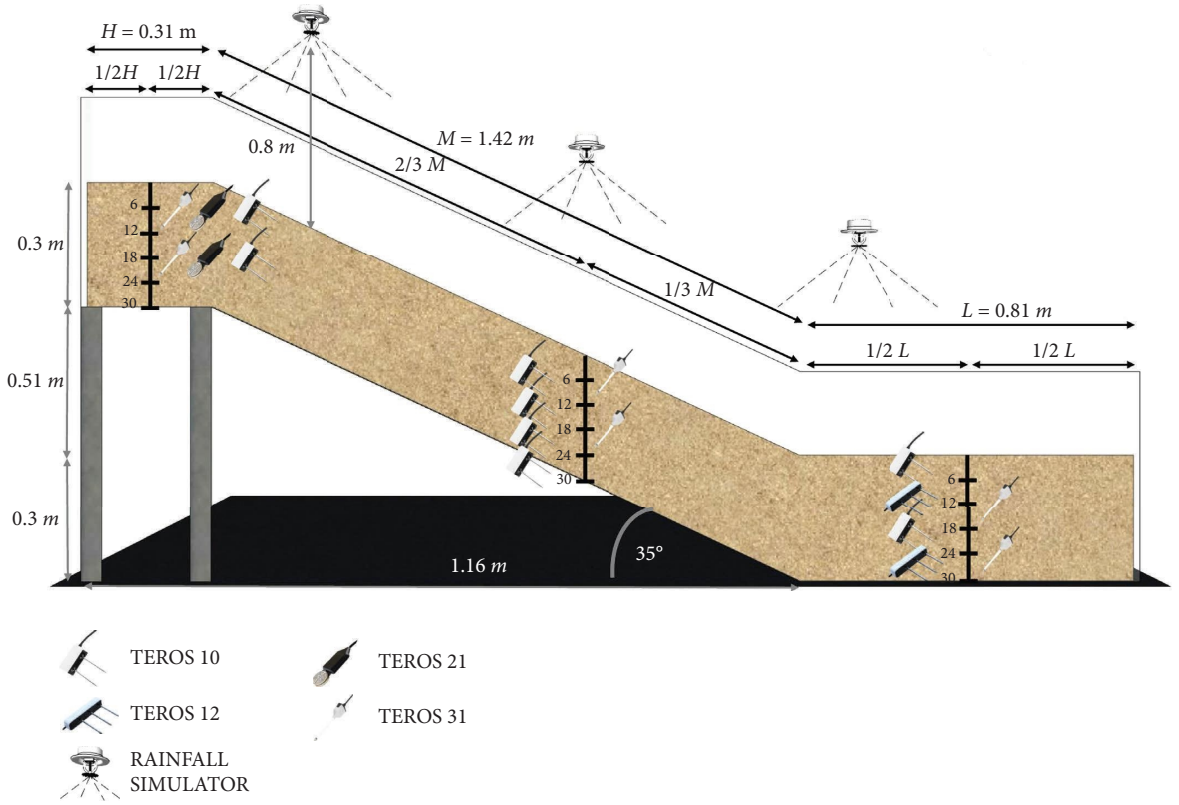

Figure 3: Positions of the embedded water-related sensors in the small-scale landslide model (modified according to Pajalic et al. [31]).

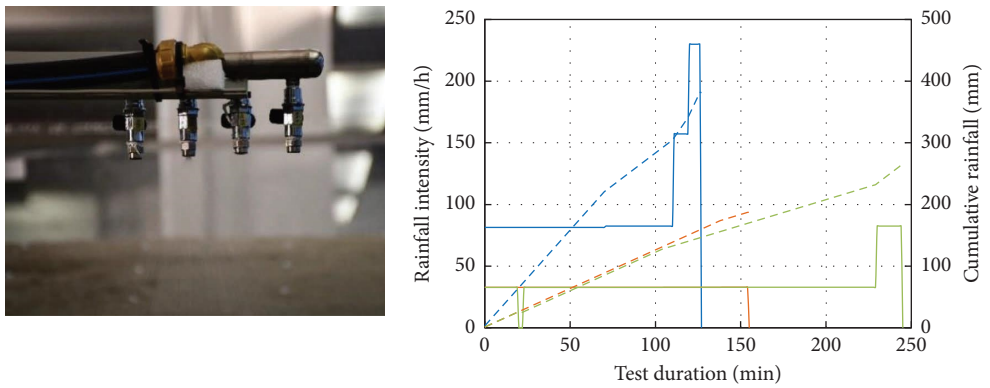

(a) (b)

Figure 4: (a) Detail of the sprinkler branch with axial-flow full-cone nozzles; (b) simulated rainfall in Test 1 (blue), Test 2 (orange), and Test 3 (green).

Table 2: Basic data of the performed tests.

Test no.	Slope angle (°)	Materials	Rainfall intensity (mm/h)	Time to initiation (min)	Test duration (min)
Test 1	35	Sand (S)	82	56	126
Test 2		Sand + 10% kaolin (SK10)	33	24	155
Test 3		Sand + 15% kaolin (SK15)	33	35	245

Soil mass failed and small rotational landslide occurred at the toe of the slope. Following this, further cracking and retrogressive sliding developed up to the top of the slope, when the test was terminated. The time from the rainfall start to the first signs of instability in the slope foot was relatively long—56 minutes (Figure 5(a)), while the retrogressive development to the top of the slope occurred in the following 30 minutes.

Figure 5: First signs of instability (left), development of instabilities (middle), and conditions at the end of the test (right) for Test 1, Test 2, and Test 3.

In contrast, in Tests 2 and 3 conducted on clay-like slopes, the failure mode was completely different from that observed for sandy slope. Although reduced infiltration capacity of sand-kaolin soil mixtures necessitated using significantly lower rainfall intensities from those used on sandy slope, first signs of instability (cracks) appeared relatively quickly after the rainfall began: 24 and 35 minutes for SK10 and SK15, respectively (Figures 5(d) and 5(g)). After appearance of the first tension cracks, the further cracking development occurred towards the top of the slope without significant movements in the slope—just new cracks were opening. The new stage occurred at the moment when the groundwater level reached the slope surface in the middle part of the slope, forming small springs, and surface flows (Figures 5(e) and 5(h)). At this moment, the joint mechanism of sliding and surface erosion started with a relatively fast retrogressive instability development up to the top of the slope. The rainfall-induced slope failures in clay-like soils were not initiated at the bottom of the slope, but in the seepage area at the slope surface, more precisely in the middle part of the slope.

4.2. Volumetric Water Content Analysis. There was no homogeneous moisture distribution at the start of Test 1 due to retention characteristics of the sandy material. All sensor measurements showed slightly higher initial values of VWC at the start of the test, starting from an initial moisture content of 2% that corresponds to VWC of 0.03 m^3/m^3 at the moment of sand material preparation. The greatest difference could be seen for sensors in the lower (L) part of the

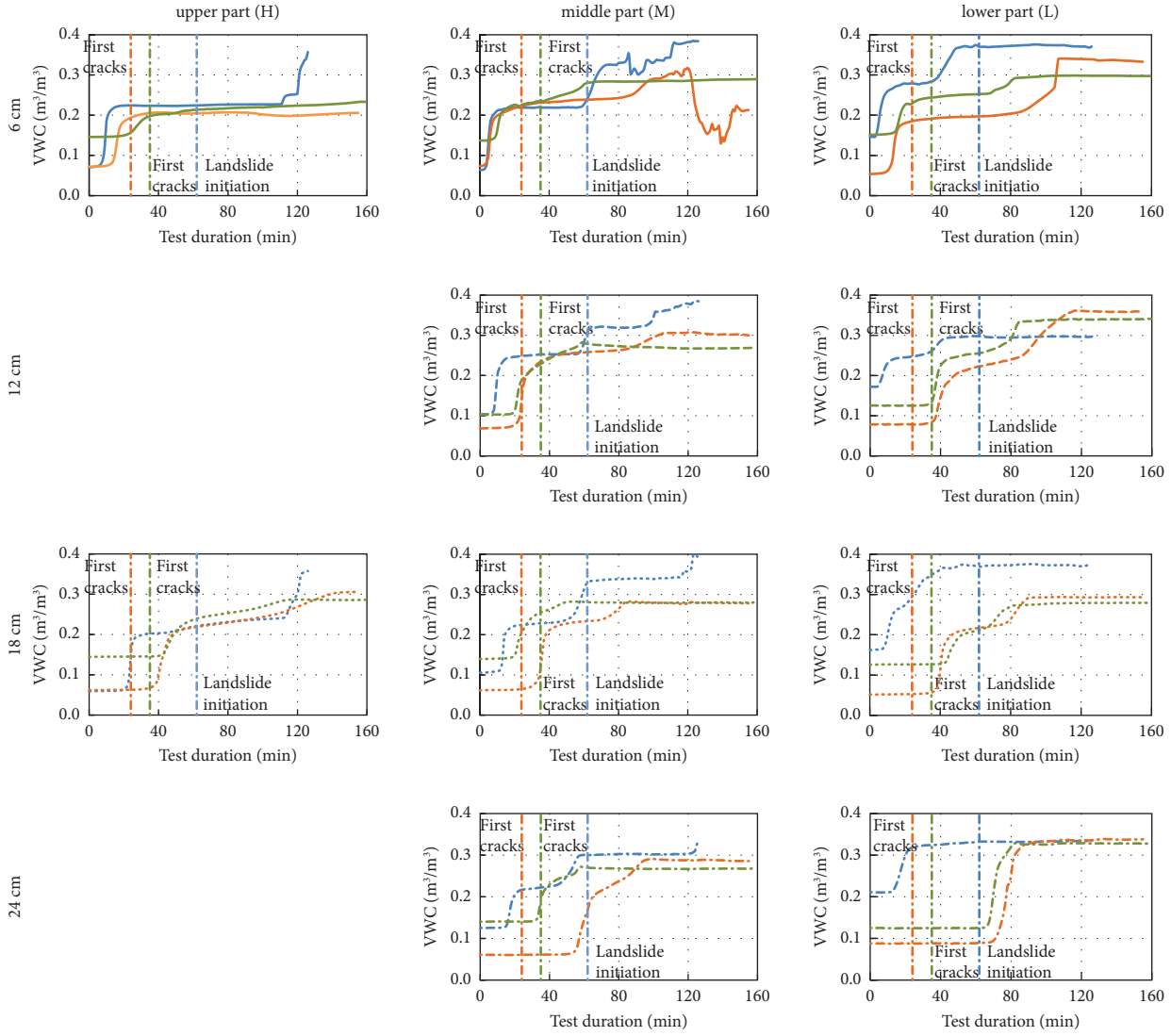

Figure 6: Volumetric water content (VWC) in Test 1 (blue), Test 2 (orange), and Test 3 (green) in the upper (H), middle (M), and lower (L) part of the slope at 6 cm, 12 cm, 18 cm, and 24 cm depth from the slope surface.

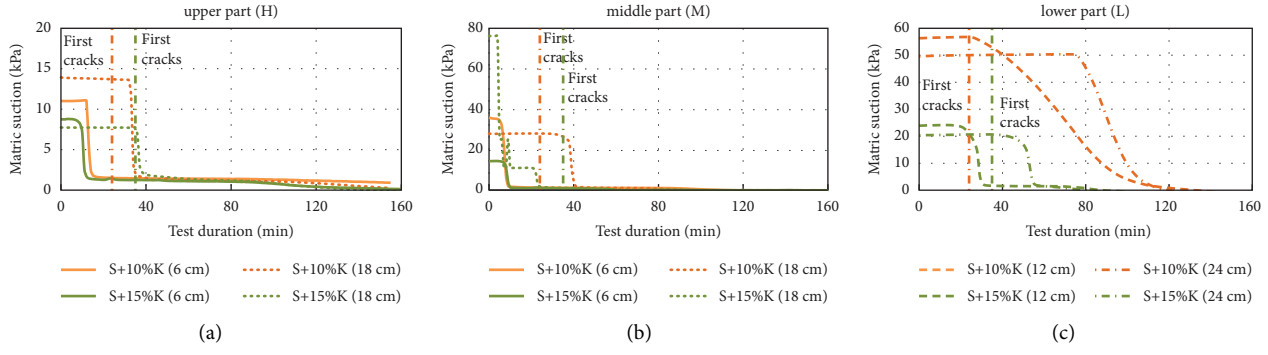

Figure 7: Matric suction in Test 2 (orange) and Test 3 (green) in (a) upper (H), (b) middle (M), and (c) lower (L) part of the slope at 6, 12, 18, and 24 cm depth from the slope surface.

slope: sensor at 6 cm depth (L-6) with 0.146 m^3/m^3 value of VWC from the one at 24 cm depth (L-24) with 0.211 m^3/m^3. This nonhomogeneous water content distribution in the model at the beginning of the test could be explained by the hydraulic properties of the sand and the time of model construction, which extended over several days, during

which evaporation and internal redistribution of the water content took place simultaneously.

The first increase of VWC occurred very quickly after the start of the test and near the slope surface at the beginning of the test, with the shallower sensors (at 6 cm depth) responded earlier than those deeper within the slope profile (at 12, 18, and 24 cm depth, respectively) in all three parts of the slope and in all three tests. The increase in soil moisture was observed with the advancement of the wetting front during the infiltration of the rainfall. For example, in the lower (L) part of the slope, in Test 1, 3 minutes after the rainfall started for the sensor at 6 cm depth and after 6, 8, and 13 minutes for the sensor at 12, 18, and 24 cm depth, respectively. In Test 2, increase in soil moisture was observed at 9, 30, 36, and 70 minutes after the rainfall started for the sensor at 6, 12, 18, and 24 cm depth, respectively. In Test 3, the increase in soil moisture started at 13, 34, 43, and 66 minutes after the rainfall started for the sensor at 6, 12, 18, and 24 cm depth, respectively.

The VWC readings became constant at a certain point in the test, indicating that saturated conditions had been reached. Measurement results showed that the VWC of the sandy slope in the lower (L) part of the slope had almost reached the saturated value indicating that the entire lower section of the model was completely submerged at the moment of landslide initiation. However, in case of clay-like slopes, measured values show that the VWC increased even after the appearance of the first cracks.

The rise in the GWL continued until the water level reached the surface of the slope foot, first in Test 1, then, for the clay-like slope, for Test 3 and Test 2, respectively. Then, the highest drainage pipe was opened to maintain the GWL at the soil surface in the lower (L) part of the model.

In the middle (M) part of the slope, the GWL raised but did not reach the maximum value for some time, and there is a steady-state flow. Rise of the GWL in this part of the slope was noticeable at the deepest sensors (M-24), after about 15, 32, and 51 minutes of rainfall, in Test 1, Test 3, and Test 2, respectively.

The measurement results of the VWC values in Test 1 showed that the GWL reached the deeper sensors first and then also the shallower ones, more precisely the sensor at 24, 18, 12, and 6 cm after about 23, 39, 41, and 49 minutes, respectively, in the lower (L) part of the slope. Based on the visual observations, the GWL reached the ground surface in the L part of the model and the foot of the slope was submerged after 51 minutes. This time is 2 minutes after the GWL reached the shallowest sensor, L-6, which fits quite closely. Failure in the form of small rotational slide in the foot of the slope occurred 56 minutes after the test started, 5 minutes after the lower (L) part of the slope was submerged, and there after the failure progressed retrogressively towards the top of the slope. The sensors in the middle (M) part of the slope also showed that the GWL reached sensors at 24, 18, 12, and 6 cm at 59, 64, 67, and 74 min after the start of the test, respectively. Data collected at monitoring point M-6 started to fluctuate at approximately 80th minute of the test that corresponds to the observed displacements occurred in this part of the slope indicated by visual observation.

Interpretation of the VWC sensor readings in the clay-like slopes in Test 2 and Test 3 was difficult and did not show the rise in the GWL as accurately as in sandy slope. In clay-like slopes, the rise of the GWL was not only related to infiltration of rainfall, but several mechanisms acted simultaneously instead: rain infiltration affected not only the moisture change but also the change in soil's weight, as a result of which cracks appeared through which preferential flow occurred. Seepage face formed in the lower part of the slope and surficial flow toward the lower part of the model began. Obviously, there was no clear relationship between constant VWC readings and GWL conditions for the case of clay-like slopes. In Test 2, sensor at 24, 18, 12, and 6 cm showed WVC constant value after about 86, 89, 115, and 106 minutes, respectively, after the test started in the lower (L) part of the slope, and in the middle (M) part of the slope, after about 96, 84, 106, and 111 minutes, respectively. In Test 3, sensor at 24, 18, 12, and 6 cm located in the lower (L) part of the slope showed a constant WVC value after about 81, 80, 83, and 82 minutes after the start of the test, respectively. For the middle (M) part of the slope, the same was observed after about 59, 51, 59, and 63 minutes, respectively.

4.3. Matric Suction Analysis. In Test 1, on the sandy slope with a relatively high hydraulic conductivity, the VWC increased until the full saturation in the deepest part of the slope, due to infiltration, forming the water table. Once this was established, a flow down the slope started resulting in a rapid rise in the GWL in the lower (L) part of the slope. This resulted in an increase in pore water pressure, a decrease in soil shear strength, failure, and further retrogressive slides to the top of the slope. Soil water potential sensors were not installed in the test on clean sand.

In Test 2 and 3, on slope made of a sand-kaolin mixture with lower hydraulic conductivity and relatively higher retention capacity, a significant increase in saturation degree occurred in the surface layer first, causing an increase in the weight of the surface layer, formation of cracks and shallow instabilities in the middle part of the slope, without observation of significant movements. The cracks opening allowed water to penetrate in deeper layers and form separated saturated zones in the slope, but with a matric suction maintained in most parts of the slope. In some isolated local zones near the existing cracks, the GWL raised to the surface, causing springs and surface flows.

The tensiometers in the upper (H) and middle (M) parts of the slope recorded a strong decrease of the matric suction, first in the shallower part (at 6 cm depth) and then also in the deeper part (at 18 cm depth). In the lower (L) part of the slope, there was also a sudden decrease of the matric suction first in the shallower layer (at 12 cm depth) L-12 and then in the deeper layer (at 24 cm depth) L-24. The exception was Test 2, where instead of mini tensiometer T31, a large tensiometer T32 was used. Due to its large volume and

design, which is generally intended for field measurements, the T32 reacts more slowly to changes in pore water pressure and therefore indicates a slow reduction in soil suction, in contrast to soil moisture measurements.

In Test 2, at the upper (H) part of the slope, only 10 minutes after the start of the test, the tensiometers at 6 cm depth H-6 started to record larger changes in suction, from 11.1 kPa to 1.6 kPa in the 16th minute. The matric suction value in the H-18 point showed a decrease after 32 minutes, from 13.5 to 1.6 kPa in the 39th minute. It took only 6 minutes for the matric suction to drop from 35.1 to 1.7 kPa in the M-6 point. The matric suction in the M-18 point remained relatively high (27.5 kPa) until the 32nd minute of the test, when a decrease to 1.9 kPa was observed in the following 9 minutes. Positive pore water pressure was recorded after 111 and 93 minutes in the M-6 and M-18 point, respectively. At the lower (L) part of the slope, a slower decrease in suction was recorded, and water pressure remained positive until 132nd and 119th minute in the L-12 and L-24 point, respectively.

In Test 3, tensiometer in the H-6 observed sudden change in matric suction 6 minutes after the start of the test, from 8.7 kPa to 1.4 kPa in the 15th minute of the test. The matric suction value in the H-18 point started to decrease after 35 minutes, from 7.7 to 2.1 kPa in the 39th minute of the test. It took only 7 minutes for the matric suction to rapidly decrease from 14.3 to 1.1 kPa in the M-6 point. The matric suction value in the M-18 point started to decrease only 3 minutes after the start of the test, from 76.2 to 11 kPa in the 7th minute. Positive pore water pressure was recorded after 98 and 89 minutes at the M-6 and M-18 cm point, respectively. A sudden decrease in matric suction in the L-12 point was observed 18 minutes after the start of the test, from 24.1 to 1.8 kPa in the 32nd minute. The matric suction in the L-24 point remained constant (20.7 kPa) until the 37th minute of the test, when a decrease to 1.8 kPa was observed in the following 20 minutes. Positive water pressure was reached after 87 and 79 minutes of the test in the L-12 and L-24 point, respectively.

Finally, it should be emphasised that there are some differences and difficulties in reconstructing infiltration and GWL rise with the two types of sensors, i.e., soil moisture sensors and tensiometers. While poor preconditioning of tensiometers can result in slow sensor response and long calibration times, volumetric deformation of soils with fine-grained particles during soil moisture increase, as is the case with sand-kaolin mixtures, can also affect VWC readings, making it difficult to detect fully saturated conditions in the soil.

5. Conclusion

Laboratory tests on physical models of landslides are of great importance because they allow the observation and measurement of phenomena closely related to the landslide mechanisms. For this reason, model platform designed and built at the Faculty of Civil Engineering, University of Rijeka, was successfully used to investigate small-scale physical models of slope failures built in different soil types exposed to artificial rainfall.

In this paper, the results of the conducted tests on homogeneous slopes built of three different soil types at the same slope angle of 35°, exposed to artificial rainfall were presented. The observed failure mechanisms were described and explained, focusing on measurements of volumetric water content and matric suction. In the sandy slope, rise of the GWL triggered sliding at the toe of the slope and further retrogressive sliding and cracking developed towards the top of the slope. Meanwhile, in the less permeable clay-like slopes, formation of soil cracks was observed very quickly after the onset of rainfall. However, no significant movements were observed until a seepage face was formed in the lower part of the slope and surface flow towards the lower part of the model began; only when the matric suction was almost completely dissipated, a combined effect of surface erosion and sliding lead to significant movements in the slope model. In general, the observed hydromechanical responses indicate that the matric suction played an important role in the performance of slope models built in sand-kaolin mixtures.

The rainfall infiltration and the GWL rise in the sandy slope model can be interpreted from the volumetric water content measurements. In this case, the instability occurred due to the groundwater rise, while no significant movements were observed during the transient infiltration stage. In the clay-like slopes, several processes occur simultaneously (from water infiltration to surficial flow and flow through cracks) and the interpretation of the slope's hydromechanical response is not so simple.

However, the presented results need to be deeply investigated with respect to the evolution of the water content profile and the changes in displacements which were also carried out in tests. Furthermore, numerical analyses are also recommended to better understand the processes and initiation of landslides in small-scale slope models. Comparison of these experimental results with numerical model results could provide a concept of a moisture content-based warning system.

Data Availability

Data can be found at https://modland.uniri.hr/?lang=hr.

Conflicts of Interest

The authors declare that they have no conflicts of interest.

Acknowledgments

This research was funded by the Croatian Science Foundation under the Project IP-2018-1503 Physical modelling of landslide remediation constructions behaviour under static and seismic actions (ModLandRemSS). The part of the laboratory equipment used for laboratory testing was provided in the frame of the Project Research Infrastructure for Campus-based Laboratories at the University of Rijeka, co-funded in a part by the Ministry of Science, Education, and

Sports of the Republic of Croatia and the European Regional Development Fund (ERDF). This work has been supported by the International Consortium on Landslides under the IPL-256 project. This work has been partially supported by the University of Rijeka project uniri-mladi-tehnic-22-62. These supports are gratefully acknowledged. The authors would like to thank Vedran Jagodnik, Nina Čeh, and Juraj Stella for their help in conducting the tests.

References

[1] D. M. Cruden and D. J. Varnes, "Landslide type and processes," in *Landslides: Investigation and Mitigation*, A. K. Turner and R. L. Schuster, Eds., vol. 247, pp. 36–75, Special Report, Washington, DC, USA, 1996.

[2] D. Petley, "Global patterns of loss of life from landslides," *Geology*, vol. 40, no. 10, pp. 927–930, 2012.

[3] N. Casagli, S. Dapporto, M. L. Ibsen, V. Tofani, and P. Vannocci, "Analysis of the landslide triggering mechanism during the storm of 20th–21st November 2000, in Northern Tuscany," *Landslides*, vol. 3, no. 1, pp. 13–21, 2006.

[4] L. Cascini, G. Sorbino, S. Cuomo, and S. Ferlisi, "Seasonal effects of rainfall on the shallow pyroclastic deposits of the Campania region (southern Italy)," *Landslides*, vol. 11, no. 5, pp. 779–792, 2014.

[5] P. Marino, G. F. Santonastaso, X. Fan, and R. Greco, "Prediction of shallow landslides in pyroclastic-covered slopes by coupled modeling of unsaturated and saturated groundwater flow," *Landslides*, vol. 18, no. 1, pp. 31–41, 2021.

[6] J. Peranić, S. Mihalić Arbanas, and Ž. Arbanas, "Importance of the unsaturated zone in landslide reactivation on flysch slopes: observations from Valići Landslide, Croatia," *Landslides*, vol. 18, no. 12, pp. 3737–3751, 2021.

[7] S. R. Zhu, L. Z. Wu, and X. L. Song, "An improved matrix split-iteration method for analyzing underground water flow," *Engineering with Computers*, 2022.

[8] S. Zhu, L. Wu, P. Cheng, and J. Zhou, "Application of modified iterative method to simulate rainfall infiltration in unsaturated soils," *Computers and Geotechnics*, vol. 148, Article ID 104816, 2022.

[9] K. Kutara and H. Ishizuka, "Seepage flow in the embankment and stability of slope during rain (in Japanese)," *Tsuchi to Kiso*, vol. 13, no. 3, p. 1330, 1982.

[10] H. Oka, "Impacts by the "artificial landslide": re examine the rage of nature (in Japanese)," *Kagaku Asahi*, vol. 32, no. 1, pp. 152-153, 1972.

[11] O. Hunger and N. R. Morgenstern, "Experiments on the flow behaviour of granular materials at high velocity in an open channel," *Géotechnique*, vol. 34, no. 3, pp. 405–413, 1984.

[12] N. Yagi, R. Yatabe, and M. Enoki, "Laboratory and field experiments on prediction method of occurring time of slope failure due to rainfall," *Journal of Japan Landslide Society*, vol. 22, no. 1, p. 71, 1985.

[13] D. Eckersley, "Instrumented laboratory flowslides," *Géotechnique*, vol. 40, no. 3, pp. 489–502, 1990.

[14] T. Kimura, "Failure of fills due to rainfall," *Centrifuge*, vol. 24, pp. 509–516, 1991.

[15] W. A. Take, M. D. Bolton, P. C. P. Wong, and F. J. Yeung, "Evaluation of landslide triggering mechanisms in model fill slopes," *Landslides*, vol. 1, no. 3, pp. 173–184, 2004.

[16] R. M. Iverson, "Scaling and design of landslide and debris-flow experiments," *Geomorphology*, vol. 244, pp. 9–20, 2015.

[17] G. Wang and K. Sassa, "Pore-pressure generation and movement of rainfall-induced landslides: effects of grain size and fine-particle content," *Engineering Geology*, vol. 69, no. 1-2, pp. 109–125, 2003.

[18] H. Moriwaki, T. Inokuchi, T. Hattanji, K. Sassa, H. Ochiai, and G. Wang, "Failure processes in a full-scale landslide experiment using a rainfall simulator," *Landslides*, vol. 1, no. 4, pp. 277–288, 2004.

[19] A. Tohari, M. Nishigaki, and M. Komatsu, "Laboratory rainfall-induced slope failure with moisture content measurement," *Journal of Geotechnical and Geoenvironmental Engineering*, vol. 133, pp. 575–587, 2007.

[20] L. Olivares, E. Damiano, R. Greco et al., "An instrument flume to investigate the mechanics of rainfall-induced landslides in unsaturated granular soils," *Geotechnical Testing Journal*, vol. 32, no. 2, pp. 108–118, 2009.

[21] R. Greco, A. Guida, E. Damiano, and L. Olivares, "Soil water content and suction monitoring in model slopes for shallow flowslides early warning applications," *Physics and Chemistry of the Earth, Parts A/B/C*, vol. 35, no. 3-5, pp. 127–136, 2010.

[22] L. Montrasio, L. Schilirò, and A. Terrone, "Physical and numerical modelling of shallow landslides," *Landslides*, vol. 13, no. 5, pp. 873–883, 2016.

[23] E. Damiano, R. Greco, A. Guida, L. Olivares, and L. Picarelli, "Investigation on rainwater infiltration into layered shallow covers in pyroclastic soils and its effect on slope stability," *Engineering Geology*, vol. 220, pp. 208–218, 2017.

[24] A. Chueasamat, T. Hori, H. Saito, T. Sato, and Y. Kohgo, "Experimental tests of slope failure due to rainfalls using 1g physical slope models," *Soils and Foundations*, vol. 58, no. 2, pp. 290–305, 2018.

[25] G. Spolverino, G. Capparelli, and P. Versace, "An instrumented flume for infiltration process modeling, landslide triggering and propagation," *Geosciences*, vol. 9, no. 3, p. 108, 2019.

[26] K. Lee, J. Suk, H. Kim, and S. Jeong, "Modeling of rainfall-induced landslides using a full-scale flume test," *Landslides*, vol. 18, no. 3, pp. 1153–1162, 2021.

[27] K.-H. Yang, T. S. Nguyen, H. Rahardjo, and D.-G. Lin, "Deformation characteristics of unstable shallow slopes triggered by rainfall infiltration," *Bulletin of Engineering Geology and the Environment*, vol. 80, no. 1, pp. 317–344, 2021.

[28] Ž. Arbanas, S. Pajalić, V. Jagodnik et al., "Development of physical model of landslide remedial constructions' behaviour," in *Proceedings of the 4th Regional Symposium on Landslides in the Adriatic – Balkan Region*, pp. 103–108, Sarajevo, Bosnia and Herzegovina, June 2019.

[29] Ž. Arbanas, V. Jagodnik, and J. Peranić, "Physical model of rainfall induced landslide in flume test: preliminary results," in *Proceedings of the 4th European Conference on Physical Modelling in Geotechnics - ECPMG 2020*, pp. 115–122, Luleå, Sweden, September 2020.

[30] V. Jagodnik, J. Peranić, and Ž. Arbanas, "Mechanism of landslide initiation in small-scale sandy slope triggered by an artificial rain," in *Understanding and Reducing Landslide Disaster Risk: Volume 6 Specific Topics in Landslide Science and Applications*, Ž. Arbanas, P. T. Bobrowsky, K. Konagai, K. Sassa, and K. Takara, Eds., Springer International Publishing, Cham, pp. 177–184, 2021.

[31] S. Pajalić, J. Peranić, S. Maksimović, N. Čeh, V. Jagodnik, and Ž. Arbanas, "Monitoring and data analysis in small-scale landslide physical model," *Applied Sciences*, vol. 11, p. 5040, 2021.

[32] J. Peranić, V. Jagodnik, N. Čeh, S. Pajalić, P. Jagodnik, and Ž. Arbanas, Edited by M. Rahman and M. Jaksa, Eds., in *Proceedings of the 20th International Conference on Soil Mechanics and Geotechnical Engineering* Sydney, Australia, November 2022.

[33] N. Bezak, J. Peranić, M. Mikoš, and Ž. Arbanas, "Evaluation of hydrological rainfall loss methods using small-scale physical landslide model," *Water*, vol. 14, no. 17, p. 2726, 2022.

[34] Ž. Arbanas, J. Peranić, V. Jagodnik, N. Čeh, S. Pajalić, and M. Vivoda Prodan, "Behaviour of sandy and clayey slopes exposed to artificial rain in small-scale model," in *Proceedings of the International Conference on Physical Modelling in Geotechnics ICPMG2022*, pp. 712–715, Daejeon, Korea, September 2022.

[35] J. Peranić, V. Jagodnik, N. Čeh, S. Pajalić, P. Jagodnik, and Ž. Arbanas, "Landslide initiation in small-scale sandy and clayey slopes exposed to artificial rain," in *Proceedings of the 20th International Conference on Soil Mechanics and Geotechnical Engineering*, pp. 1075–1080, Sydney, Australia, May 2022.

[36] N. Čeh, J. Peranić, V. Jagodnik, S. Pajalić, M. Vivoda Prodan, and Ž. Arbanas, "Digital image correlation and the use of high-speed cameras for 3D displacement monitoring in 1g small-scale landslide models," in *Proceedings of the 5th ReSyLAB 'Landslide Modelling & Applications'*, pp. 181–186, Rijeka, Croatia, June 2022.

[37] M. Vivoda Prodan, J. Peranić, S. Pajalić, V. Jagodnik, N. Čeh, and Ž. Arbanas, "Mechanism of rainfall induced landslides in small-scale models built of different materials," in *Proceedings of the 5th ReSyLAB 'Landslide Modelling & Applications'*, pp. 187–192, Rijeka, Croatia, March 2022.

[38] Ž. Arbanas, J. Peranić, V. Jagodnik et al., "Impact of gravity retaining wall on the stability of a sandy slope in small-scale physical model," in *Proceedings of the 5th Regional Symposium on Landslides in Adriatic-Balkan Region*, pp. 193–200, Rijeka, Croatia, April 2022.

[39] J. Peranić, V. Jagodnik, N. Čeh, M. Vivoda Prodan, S. Pajalić, and Ž. Arbanas, "Small-scale physical landslide models under 1g infiltration conditions and the role of hydrological monitoring," in *Proceedings of the 5th ReSyLAB 'Landslide Modelling & Applications*, pp. 171–180, Rijeka, Croatia, March 2022.

[40] J. Peranić, N. Čeh, and Ž. Arbanas, "The use of soil moisture and pore-water pressure sensors for the interpretation of landslide behavior in small-scale physical models," *Sensors*, vol. 22, no. 19, p. 7337, 2022.

[41] R. S. Ladd, "Preparing test specimens using undercompaction," *Geotechnical Testing Journal*, vol. 1, pp. 16–23, 1978.

[42] G. F. Wieczorek and J. B. Snyder, *Monitoring Slope Movements, Geological Monitoring*, Geological Society of America, Boulder, Colorado, 2009.

[43] C. C. Huang and L. L. Chien, "Simulation of subsurface flows associated with rainfall-induced shallow slope failures," *Journal of GeoEngineering*, vol. 8, pp. 101–111, 2013.

[44] L. Z. Wu, Y. Zhou, P. Sun, J. S. Shi, G. G. Liu, and L. Y. Bai, "Laboratory characterization of rainfall-induced loess slope failure," *Catena*, vol. 150, pp. 1–8, 2017.

[45] A. Zanutta, P. Baldi, G. Bitelli, and M. Cardinali, "Qualitative and quantitative photogrammetric techniques for multi temporal landslide analysis," *Annals of Geophysics*, vol. 49, no. 4-5, pp. 4-5, 2009.